

Nautilus: Locality-aware Autoencoder for Scalable Mesh Generation

YUXUAN WANG*, Nanyang Technological University, Singapore

XUANYU YI*, Nanyang Technological University, Singapore

HAOHAN WENG*, Tencent Hunyuan, China

QINGSHAN XU, Nanyang Technological University, Singapore

XIAOKANG WEI, The Hong Kong Polytechnic University, Hong Kong, China

XIANGHUI YANG, Tencent Hunyuan, China

CHUNCHAO GUO, Tencent Hunyuan, China

LONG CHEN, Hong Kong University of Science and Technology, Hong Kong, China

HANWANG ZHANG, Nanyang Technological University, Singapore

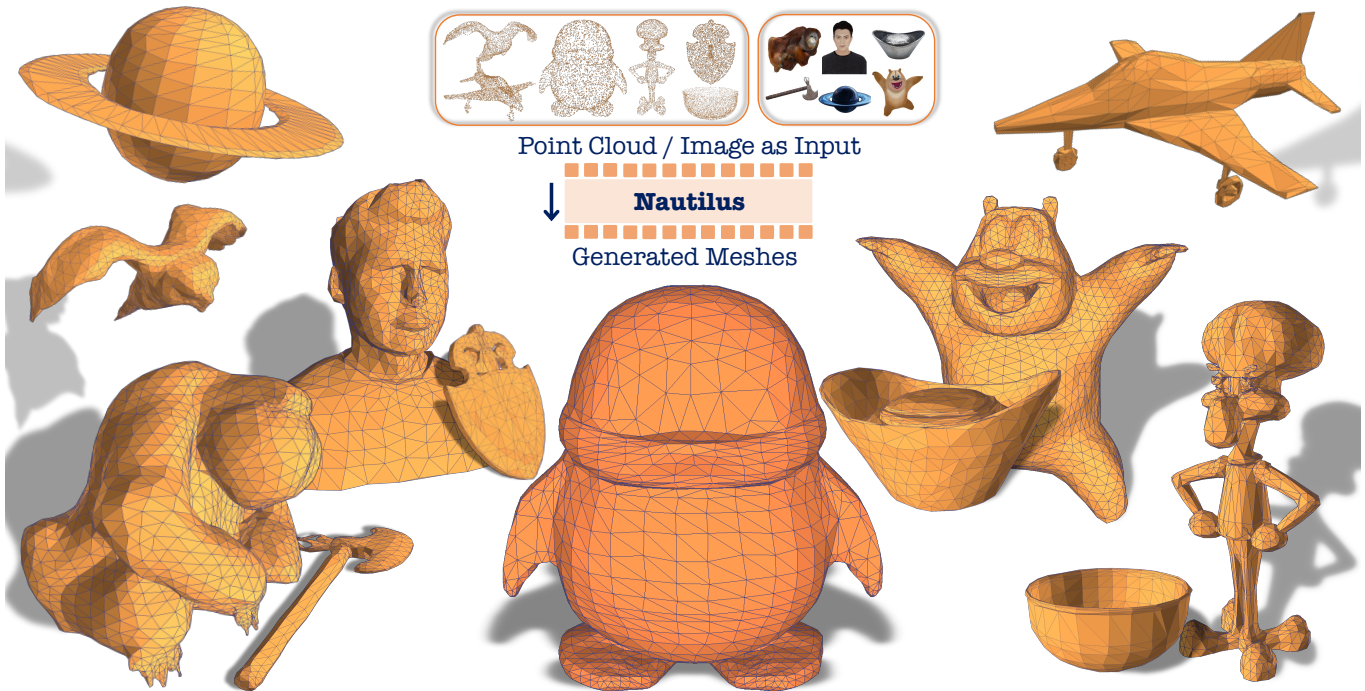


Fig. 1. Capability highlight of our **Nautilus**: Given a point cloud (e.g., the *bird*, *aircraft*, *penguin*, *Sqog*, *shield*, and *bowl* shown in the figure) or a single image (e.g., the *gorilla*, *ax*, *man*, *planet*, *sycee*, and *bear* shown in the figure) as input, **Nautilus** enables the direct generation of aesthetic, artist-like mesh assets conditioned on the input. By explicitly modeling and leveraging locality, it delivers superior generation quality and unprecedentedly detailed topologies.

Triangle meshes are fundamental to 3D applications, enabling efficient modification and rasterization while maintaining compatibility with standard rendering pipelines. However, current automatic mesh generation methods typically rely on intermediate representations that lack the continuous surface quality inherent to meshes. Converting these representations into meshes produces dense, suboptimal outputs. Although recent autoregressive approaches demonstrate promise in directly modeling mesh vertices and faces, they are constrained by the limitation in face count, scalability,

and structural fidelity. To address these challenges, we propose Nautilus, a locality-aware autoencoder for artist-like mesh generation that leverages the local properties of manifold meshes to achieve structural fidelity and efficient representation. Our approach introduces a novel tokenization algorithm that preserves face proximity relationships and compresses sequence length through locally shared vertices and edges, enabling the generation of meshes with an unprecedented scale of up to 5,000 faces. Furthermore, we develop a Dual-stream Point Conditioner that provides multi-scale geometric guidance, ensuring global consistency and local structural fidelity by capturing fine-grained geometric features. Extensive experiments demonstrate that Nautilus significantly outperforms state-of-the-art methods in both fidelity and scalability. The project page is at <https://nautilusmeshgen.github.io>.

Authors' Contact Information: Yuxuan Wang*, Nanyang Technological University, Singapore; Xuanyu Yi*, Nanyang Technological University, Singapore; Haohan Weng*, Tencent Hunyuan, China; Qingshan Xu, Nanyang Technological University, Singapore; Xiaokang Wei, The Hong Kong Polytechnic University, Hong Kong, China; Xianghui Yang, Tencent Hunyuan, China; Chuncho Guo, Tencent Hunyuan, China; Long Chen, Hong Kong University of Science and Technology, Hong Kong, China; Hanwang Zhang, Nanyang Technological University, Singapore.

CCS Concepts: • Computing methodologies → Mesh geometry models; Mesh models; Shape inference.

1 Introduction

Triangle meshes, composed of interconnected triangles that approximate arbitrary topology in space, are fundamental to 3D applications [Dai and Nießner 2019; Hong et al. 2024; Siddiqui et al. 2024]. Their structure enables efficient modification and rasterization, ensuring compatibility with standard rendering pipelines. Currently, creating high-quality meshes primarily relies on skilled 3D artists with tools such as Blender, making the process labor-intensive and difficult to scale. Therefore, automating high-quality mesh generation is essential to meet the demands of modern 3D applications.

However, current automatic approaches mainly adopt intermediate representations such as Voxels [Brock et al. 2016; Ren et al. 2024; Wu et al. 2016], Point cloud [Luo and Hu 2021; Nichol et al. 2022; Zhou et al. 2021], NeRF [Hong et al. 2023; Poole et al. 2022; Wang et al. 2024; Yi et al. 2024b], and 3DGS [Shen et al. 2024; Tang et al. 2025; Wang et al. 2025; Yi et al. 2024a; Zhang et al. 2024a], which inherently lack the continuous surface of the meshes. Converting these representations into meshes through marching cubes [Lorensen and Cline 1998] or Poisson reconstruction [Kazhdan et al. 2006] often yields dense, suboptimal meshes, lacking the conciseness and aesthetic of artist-created models. Even with post-processing such as remeshing [Attene and Falcidieno 2006], the generated meshes remain substantially inferior to artist-created assets, as highlighted by [Chen et al. 2024b] and [Siddiqui et al. 2024].

Very recently, a line of works has showcased the potential of directly modeling mesh structures [Chen et al. 2024a,b; Siddiqui et al. 2024] in an auto-regressive manner. Pioneered by MeshGPT [Siddiqui et al. 2024], this paradigm tokenizes mesh faces into sequences and employs a GPT-style decoder to autoregressively generate the sequences, enabling direct capture of vertex-face relationships. MeshAnything [Chen et al. 2024b] further enhanced this framework by incorporating point cloud conditioning for global geometric guidance. Through explicit modeling of mesh vertices and faces, these methods generate more concise and structurally refined meshes.

Despite these advances, current direct mesh generation still encounters several fundamental challenges: (1) Existing methods often struggle to maintain local structure fidelity [Chen et al. 2024b,c; Weng et al. 2024], as shown in Fig. 2(a), exhibiting manifold defects such as surface holes, overlapping faces, and missing components, especially when dealing with complex topologies. (2) Moreover, existing methods are typically limited to modeling meshes with fewer than 1,600 faces, which significantly constrains their ability to capture the intricate topological details required for industrial applications, as illustrated in Fig. 2(b).

Drawing from 3D artists’ creation with precise structure and seamless transitions, we conjecture that the crux arises from inadequate modeling of manifold mesh **locality**—where adjacent faces share common edges and each face cluster converges at a central vertex. This locality offers two key inspirations to overcome the aforementioned challenges: (1) **Local structure preservation.** The locality ensures that the geometry of each face is directly constrained by its immediate neighbors. Thus, prioritizing local dependencies on neighbors and their topology could be crucial for faces to form precise interconnection, achieving manifoldness and structure fidelity

*These authors contributed equally to this work.

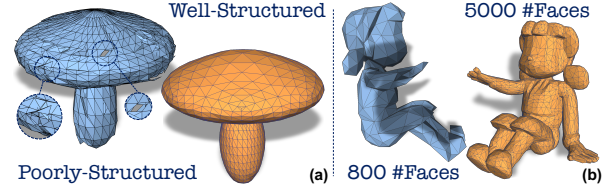


Fig. 2. Fundamental challenges in current methods. (a) Being restricted to generating meshes with fewer faces leads to the loss of fine topological details compared to higher face count meshes. (b) Struggling to preserve local structure fidelity causes manifold defects like surface holes and overlapping faces, in contrast to well-structured assets.

rather than merely approximating the shape contour. (2) **Efficient mesh representation.** Explicitly modeling the locally shared edges and vertices could significantly reduce redundancy in representation and compress the sequence, allowing the modeling of refined meshes with higher face counts and more complex topology.

To this end, we propose **Nautilus**, a locality-aware autoencoder for scalable artist-like mesh generation. First, we design a novel Nautilus-style mesh tokenization algorithm (Sec. 3.1) that preserves the proximity of neighboring faces within the sequence, laying the foundation for modeling local dependencies during generation. In particular, by leveraging the locally shared vertices and edges, it reduces the sequence length to 1/4 and allows the generation of meshes with up to an unprecedented 5,000 faces. Second, we introduce a Dual-stream Point Conditioner (Sec. 3.2) that provides multi-scale geometric guidance, ensuring global shape consistency while enhancing local structure fidelity by capturing fine-grained local geometry. Extensive experiments (Sec. 4) demonstrate that Nautilus significantly outperforms existing methods, delivering high-quality, artist-like mesh generation with intricate topology.

In summary, our key contributions are threefold:

- We pinpoint the neglect of mesh locality as a fundamental limitation in current methods of direct artist-like mesh generation.
- We propose **Nautilus**, which effectively leverages mesh locality through its novel tokenization algorithm along with dual-stream conditioning mechanism.
- We demonstrate the scalability of Nautilus through extensive experiments on a large, carefully curated dataset, showing that it achieves high-quality mesh generation with unprecedented topological complexity.

2 Related Work

Mesh Generation with Intermediate Representation. Most existing 3D generation methods create meshes through intermediate representations, including neural fields [Poole et al. 2022; Wu et al. 2024b; Yi et al. 2024b], 3DGS [Chung et al. 2023; Tang et al. 2023], and SDF [Park et al. 2019; Xu et al. 2024]. Utilizing SDS optimization [Lin et al. 2023; Poole et al. 2022; Wang et al. 2024] with pre-trained 2D models [Esser et al. 2024; Rombach et al. 2022], early approaches achieved high quality but required hours of computation per instance. Following the emergence of large-scale 3D datasets, research shifted toward feed-forward 3D models [Hong et al. 2023;

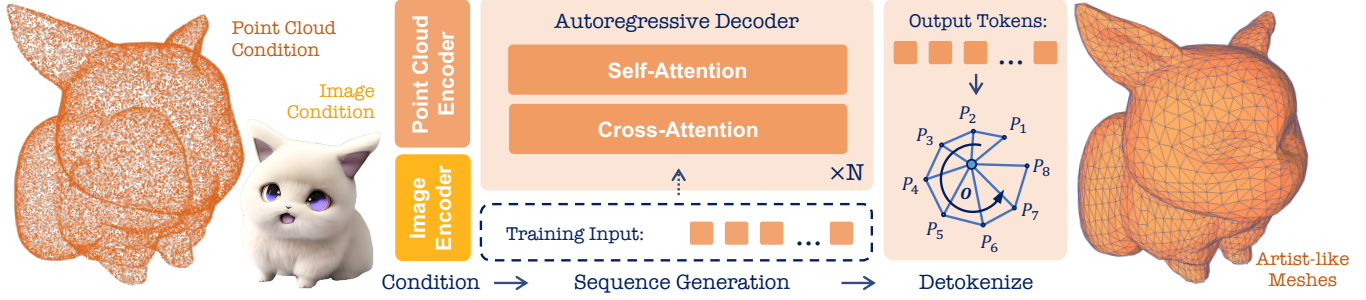


Fig. 3. The overall pipeline of **Nautilus**. Given a point cloud or image as input, its transformer decoder autoregressively generates mesh sequence tokenized by the Nautilus-style algorithm. Through detokenization, the output tokens are converted to interconnected mesh faces, constructing our generated mesh assets.

Tang et al. 2025; Yi et al. 2024a]. Pioneered by the Large Reconstruction Model (LRM), one line of work [Shen et al. 2024; Zhang et al. 2024a] demonstrated that end-to-end training with differentiable rendering and Transformer-based models [Vaswani 2017] could generate 3D assets within seconds. Another line of work [Li et al. 2024b; Wu et al. 2024a; Zhang et al. 2024b] employs 3D-native latent diffusion with volumetric representation, encoding 3D assets into compressed latent spaces for generation through diffusion steps. However, these methods require decent post-processing [Attene and Falcidieno 2006; Lorensen and Cline 1998] and often produce overly dense or over-smooth meshes.

Direct Mesh Generation. Compared to methods using intermediate representations, direct mesh generation approaches explicitly model mesh topology, producing more concise and structurally coherent meshes without post-conversion steps. Although pioneering works such as PolyGen [Nash et al. 2020] and PolyDiff [Alliegro et al. 2023] demonstrated promise, their applications remained limited to single-category datasets. Recent advances in autoregressive approaches, notably MeshGPT [Siddiqui et al. 2024], introduced mesh tokenization with VQ-VAE [Van Den Oord et al. 2017] compression for direct mesh generation under topology supervision. Subsequent research has advanced this paradigm by exploring various architectural variants [Chen et al. 2024a; Weng et al. 2024] and extending it to conditional generation tasks [Chen et al. 2024b,c], particularly point cloud to mesh generation. However, these methods exhibit manifold defects when handling complex topologies and are limited to 1,600 faces due to the excessive length of tokenized sequence. In contrast, our Nautilus aims to achieve manifold structure fidelity through efficient locality-aware mesh representation while extending the maximum face count.

3 Nautilus

In this section, we introduce **Nautilus**, a locality-aware autoencoder for artist-like mesh generation, with the overall pipeline depicted in Fig. 3. Initially, we design a novel Nautilus-style algorithm that tokenizes artist-created meshes into sequences (Sec. 3.1), which serves as the training input of our framework. During generation, Nautilus takes either a point cloud or a single-view image as the condition inputs. For point cloud conditioning, we propose a dual-stream conditioner (Sec. 3.2) that provides both global and local geometric guidance to the autoregressive decoder, which generates

the tokenized sequence given the input condition (Sec. 3.3). For image conditioning, we integrate a pre-trained image encoder with the decoder to enable image-conditioned generation (Sec. 3.4). Finally, after detokenization, the token sequences predicted by the decoder are translated into mesh faces, constructing our generated artist-like mesh assets.

3.1 Nautilus-style Mesh Tokenization

The initial step of autoregressive mesh generation involves serializing the triangle mesh into tokens [Chen et al. 2024a,b; Siddiqui et al. 2024]. A mesh asset $M = \{f^i\}_{i=1}^N$ consists of N triangle faces f^i , each of which is represented by three vertices, $\{v_1^i, v_2^i, v_3^i\}$. By flattening the discrete 3D coordinates of each vertex, denoted as $v_j^i = \{x_j^i, y_j^i, z_j^i\}$, the mesh asset M can be serialized into an ordered sequence of coordinates, $S(M)$, with a total length of $9N$:

$$S(M) = \{v_1^1, v_2^1, v_3^1, v_1^2, v_2^2, v_3^2, \dots, v_1^N, v_2^N, v_3^N\} \quad (1)$$

However, we argue that such vanilla flattening fails to preserve spatial neighboring in the generated sequence, hindering local dependency modeling. Furthermore, its excessive sequence length limits the face count during training, hindering the model from learning complex assets with higher face numbers. To overcome these issues, we propose a Nautilus-style tokenization algorithm that maintains local neighbor proximity and reduces sequence length to 1/4 by leveraging the locally shared vertices and faces.

Nautilus Shell Representation. In tokenization, we first sort the mesh faces by their coordinates $z-y-x$ to facilitate efficient serialization. As depicted in Fig. 4(a), we divide the mesh asset into multiple **shells** for sequential generation. Each shell organizes faces around a central vertex O with an ordered sequence of surrounding vertices P , where each face is formed by O and two adjacent P as $f_{OP_1P_2}$. This organization helps maintain local mesh connectivity by explicitly encoding edge-sharing relationships between adjacent faces. Based on this shell structure, we compactly represent N faces using a sequence of $(N + 2)$ vertices, rather than the $3N$ vertices required in Eq. (1):

$$S(f_{OP_1P_2}, f_{OP_2P_3}, \dots) = \{O, P_1, P_2, P_3, \dots\} \quad (2)$$

With this representation, the *shell #1* in Fig. 4(a) can be serialized to $\{O_1, P_{1,1}, P_{1,2}, \dots, P_{1,10}, P_{1,1}\}$, which preserves the adjacency of neighboring vertices in sequence. By explicitly modeling the locally

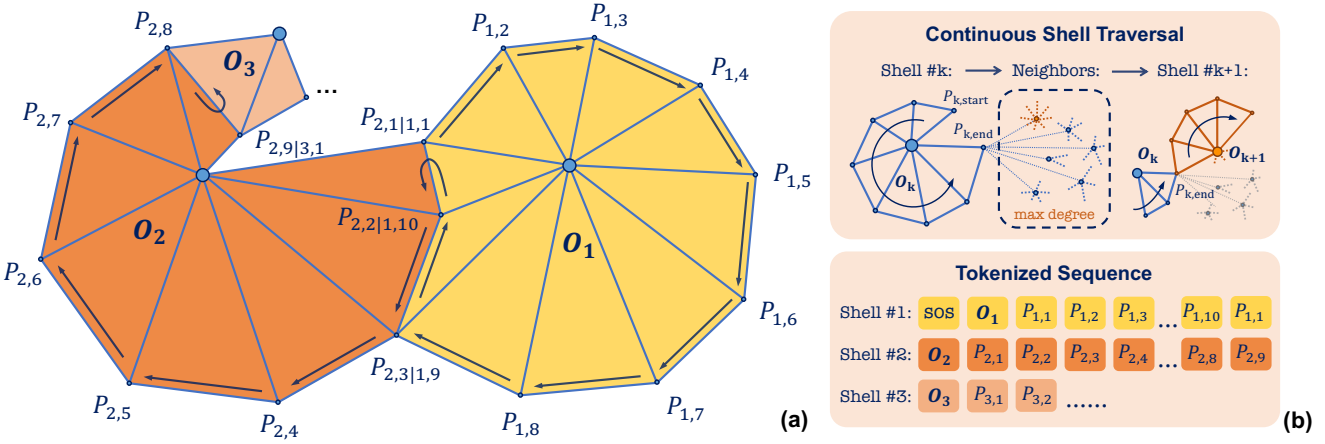


Fig. 4. The illustration of our **Nautilus-style Mesh Tokenization** algorithm. (a) The shell-structured traversal of mesh faces. (b) Top: The continuous shell traversal mechanism designed to find the center of the next shell. Bottom: The tokenized vertices sequence of the shown example.

shared vertices and faces, we could add a new face to a shell by extending the sequence with only a single vertex.

Continuous Shell Traversal. After completing the traversal of one shell, we decide the central vertex candidate for the next shell based on two insights: (1) The vertex should be close to the current shell to facilitate local, short-distance dependencies and promote coherent edge connectivity between shells. (2) The vertex should have a relatively high degree and is shared by more faces, which not only improves the compression ratio but also encourages the formation of well-connected local mesh structures. Therefore, we design the following continuous shell traversal strategy. Specifically, after completing one shell, we list all neighbor vertices of its last traversed vertex and select the neighbor with maximum degree as the center vertex of the next shell¹. Our strategy enhances the traversal continuity and spatial proximity between shells, promoting locally consistent mesh topology.

Coordinates Compression. Building upon the vertex sharing optimization in our Nautilus representation, we exploit spatial quantization and dimensional reduction techniques to achieve more compact mesh encoding. Specifically, given the 3D spatial resolution α , we can uniquely represent the discrete coordinates $(x, y, z) \in \mathbb{R}^\alpha$ as (u, v) using a scaling factor β :

$$x * \alpha^2 + y * \alpha + z = u * \beta + v \quad (3)$$

By mapping the x - y - z coordinates to u - v space, we could further compress the sequence length. With a resolution of 128 and a scaling factor of 2048, we construct a codebook of size 1024 for u and 2048 for v . Additionally, to identify the start of each shell, we extend the codebook by 1024 to separately encode the u coordinates of center vertices O , thereby distinguishing them from surrounding vertices P . This design avoids the increased sequence length introduced by the special tokens that previous work [Chen et al. 2024c; Tang et al. 2024] used for sub-sequence separation, producing our final

tokenized sequence as:

$$S(\mathbf{M}) = \{u_1^O, v_1^O, u_{1,1}^P, v_{1,1}^P, u_{1,2}^P, \dots, u_2^O, v_2^O, \dots\} \quad (4)$$

In a nutshell, our Nautilus-style tokenization provides a compact serialization to model complex mesh assets with a higher number of faces. Meanwhile, it maintains short-distance local dependencies by preserving the proximity of spatially neighboring vertices in the tokenized sequence, enhancing the fidelity of local structure. Experiments in Sec. 4 show that these advantages lead to significant improvements in scalability and generation quality. A detailed step-by-step demonstration of the tokenization process is available in *Appendix*, further illustrating its design and implementation.

3.2 Dual-Stream Point Conditioner

Following [Chen et al. 2024a,b,c], our default input condition for mesh generation is point cloud, given its easy accessibility and rich geometric information. In Nautilus, we design a dual-stream point conditioner that provides both global and local geometric guidance.

Global Point Cloud Encoder. In order to capture high-quality global features from the input point cloud, we employ the Michelangelo point cloud encoder [Zhao et al. 2024] to extract complete geometric information. As illustrated in Fig. 5, the point cloud of the entire mesh is encoded into a global latent feature, f_{glb} , which serves as the key and value in the cross-attention layer of the decoder. This global feature encapsulates the overall geometry of the mesh asset, enabling the decoder to grasp the general shape of the input point cloud and autoregressively generate an approximate mesh output that reflects the underlying structure.

Local Point Cloud Encoder. As discussed in Sec. 1, fine-grained local geometric fidelity is crucial for preserving mesh topology and structural coherence. To this end, we propose a local-aware feature extraction mechanism that aligns with our shell-based generation paradigm, providing precise geometric guidance at the vertex-fan level. As depicted in Fig. 5, we employ a PointConv [Zhang et al. 2022] module $f_{\text{loc}}(\cdot)$ to capture local geometric information from the point cloud input. Furthermore, we design a feature injection scheme

¹As depicted in Fig. 4(b), the last vertex of the shell k is located at $P_{k,end}$, therefore we choose the orange vertex with the highest degree among its neighbors as the next center O_{k+1} .

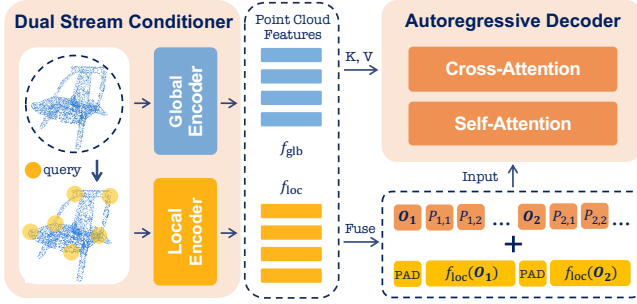


Fig. 5. Illustration of our **Dual-Stream Point Conditioner**. The Global Encoder extracts global features f_{glb} from the entire point cloud, used as key and value in cross-attention layers. The Local Encoder captures fine-grained topology information via point convolution, adding local geometric features f_{loc} to each token during generation.

that augments token embeddings with their corresponding local geometric context, inspired by ControlAR [Li et al. 2024a]. Specifically, for each vertex $P_{k,i}$ in the k -th shell, we incorporate the local feature $f_{\text{loc}}(O_k)$ extracted from its central vertex O_k into its tokens feature. For each shell’s center vertex, we construct a local neighborhood through KNN sampling of the 100 nearest points, ensuring dense coverage of local surface geometry. This tight integration with our shell-based tokenization enables progressive incorporation of local geometric constraints during generation, enhancing both topological consistency and structural fidelity.

3.3 Autoregressive Sequence Decoder

The core generator of our Nautilus is a transformer decoder that autoregressively predicts the probability of the next mesh token based on the preceding, where each layer consists of a cross-attention layer and a self-attention layer with feed-forward network.

Autoregressive Mesh Token Generation. After tokenization, the mesh generation task is simply reformulated as an autoregressive sequence prediction problem [Bai et al. 2024; Siddiqui et al. 2024; Vaswani 2017]. Using the next-token prediction paradigm, models are trained to predict each discrete coordinate $c \in \{u, v\}$ based on the conditional probability given previously generated tokens. The probability of a mesh \mathbf{M} can be expressed as:

$$p(\mathbf{M}) = \prod_{i=1}^L p(c_i | c_{<i}), \quad c_i \in \{0, 1, \dots, \alpha - 1\} \quad (5)$$

where α denotes the resolution of the discrete coordinate space, and L is the total length of the generated sequence.

Training Objective. Our decoder is trained under the next token prediction paradigm using cross-entropy loss:

$$L_{\text{CE}} = \text{CrossEntropy}(\hat{S}, S(\mathbf{M})_{>0}) \quad (6)$$

where $S(\mathbf{M})_{>0}$ represents the one-hot ground truth token sequence processed by our Nautilus-style Mesh Tokenization, excluding the initial [sos] token, and \hat{S} denotes the predicted classification logits at all positions. Consequently, the trained decoder generates tokens that our Nautilus-style tokenization algorithm can accurately detokenize and convert into output meshes.

3.4 Image Conditioned Generation

To further expand practical applications, we extend our Nautilus-style tokenization and autoregressive framework to support image-conditioned [Bai et al. 2023] mesh generation. We achieve this by leveraging the Michelangelo [Zhao et al. 2024], a pre-trained shape generation framework that aligns multiple modalities in a unified feature space. Specifically, we replace the original decoder in Michelangelo with our mesh decoder, which incorporates Nautilus-style tokenization. The decoder is trained while keeping the point cloud encoder frozen, enabling mesh generation from the unified feature space. After training, we integrate Michelangelo’s image encoder to enable single-image conditioning. Using the aligned feature space, our decoder generates high-quality meshes directly from images, as demonstrated by the experimental results in Sec. 4.

4 Experiments

4.1 Implementation Details

Our Nautilus framework is trained on a curated dataset of 311K high-quality artist-created mesh assets, which is sourced from our manually cleaned Objaverse data and self-collected data, and each containing up to 8,000 faces, with further statistics are provided in *Appendix*. For each training asset, we sample 4,096 points as input condition. Nautilus was trained on 8 NVIDIA L40 GPUs for 2 weeks and 400K steps, using Adam optimizer with a learning rate of 0.0001 and a batch size of 16. The transformer decoder includes 24 layers and contains around 500M parameters. During mesh generation, we employ probabilistic sampling with a temperature of 0.5 for stability, generating meshes of 5,000 faces in 4 minutes.

4.2 Qualitative Results

Point Cloud Condition. We compare our Nautilus with the latest open-source direct mesh generation methods [Chen et al. 2024b,c] in the point cloud conditioned generation, where EdgeRunner [Tang et al. 2024] is excluded from this comparison due to its unavailability of pretrained checkpoints. To construct the test set, we use open-source image-to-3D methods [Team 2025] to generate dense meshes and directly sample point clouds from them, ensuring that all test samples are entirely unseen during training. The selected samples present significant challenges, featuring thin structures, anisotropic faces, and intricate geometric details.

As shown in Fig.6, existing methods struggle with these challenging cases, exhibiting structural defects such as surface holes and missing components, while failing to capture fine topological details. In contrast, Nautilus generates aesthetically appealing, artist-like meshes that faithfully preserve the geometric details of the input. This performance gap stems from their inadequate locality modeling. Current tokenization approaches generate excessive sequence lengths, limiting these methods to training on simple meshes with fewer than 1,600 faces—insufficient for complex test cases. Furthermore, the limited local dependency compromises structural fidelity and increases manifold defects. Nautilus addresses these limitations by leveraging locality in both mesh tokenization and sequence generation, achieving superior quality even for complex topologies, with additional results presented in Fig.10.

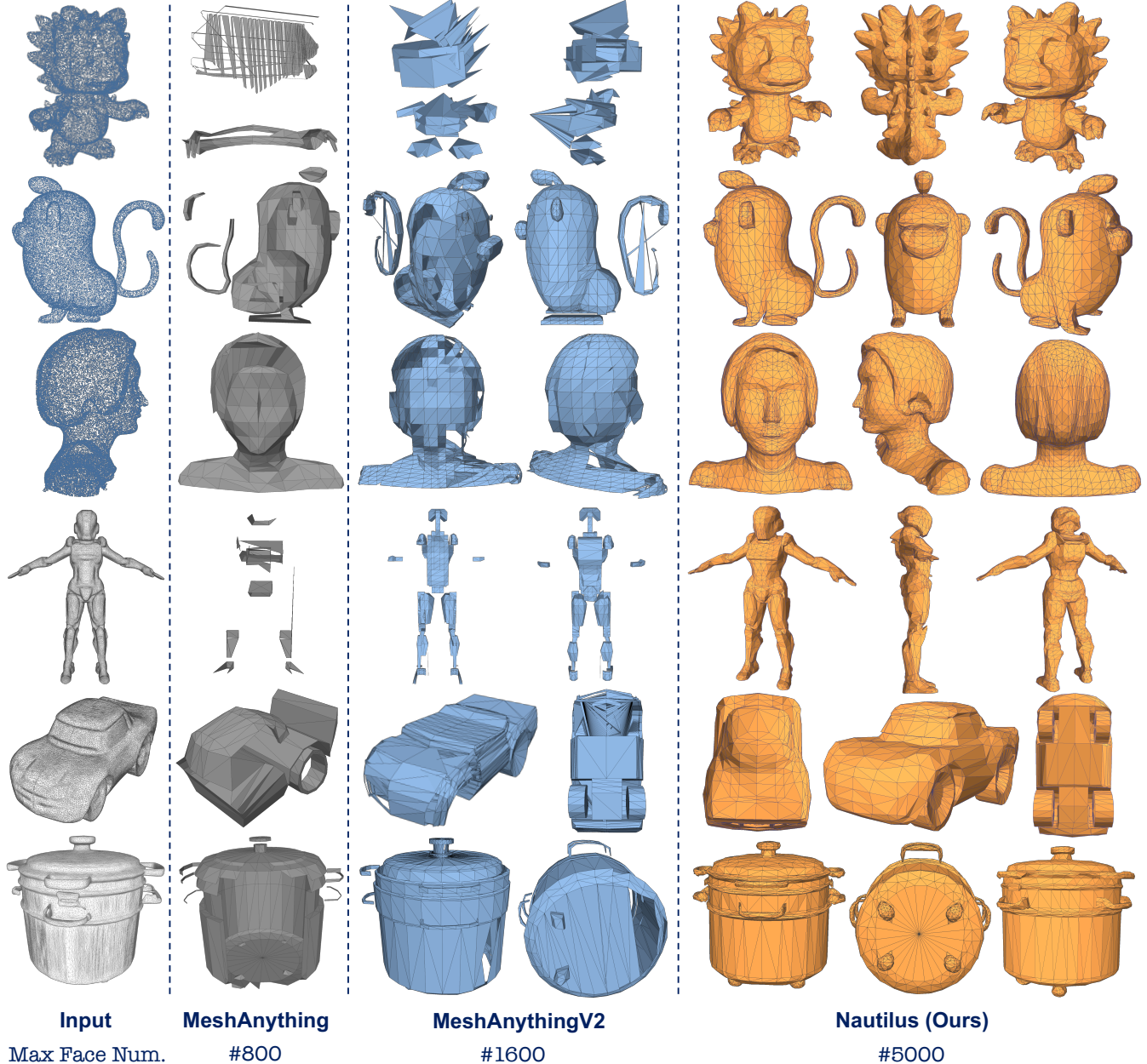


Fig. 6. Qualitative comparison on point cloud conditioned generation between Nautilus and latest open-source methods [Chen et al. 2024b,c]. For the *last three* row, the source dense meshes used to sample the input point cloud are shown in the *left-most* column.

Single-view Image Condition. In Fig. 7, we present a comparison of meshes generated from single-view images between our Nautilus and EdgeRunner [Tang et al. 2024], the only autoregressive method capable of directly conditioning on images². As shown in Fig. 7, Nautilus generates detailed, manifold meshes with sharp features that accurately match the input conditions, which highlights the

superiority of our Nautilus-style tokenization, as further validated through comparisons in Sec. 4.3.

4.3 Quantitative Results

Tokenization Algorithm. In Table 1, we compare our Nautilus-style mesh tokenization algorithm with Adjacent Mesh Tokenization (AMT) [Chen et al. 2024c] and EdgeRunner [Tang et al. 2024] in two aspects: (1) **Compression Ratio** measures the reduction in

²Note that our comparison is limited to EdgeRunner’s released samples, as their checkpoints are not publicly available.

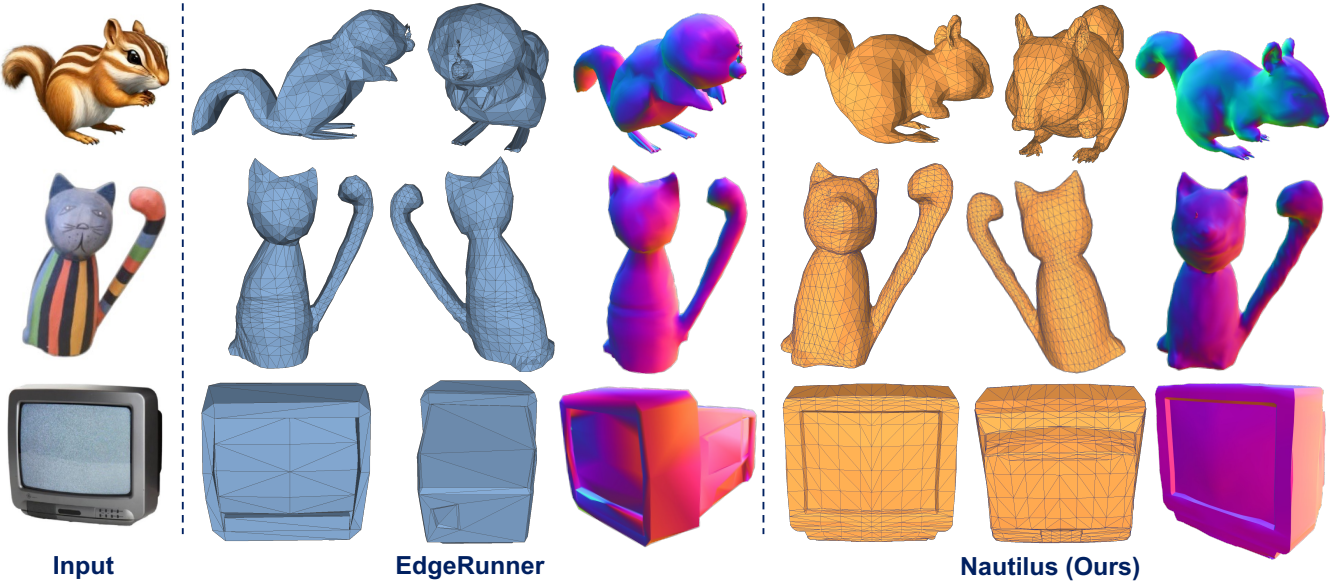


Fig. 7. Qualitative comparison on single image conditioned generation between Nautilus and EdgeRunner [Tang et al. 2024]. The results are presented with corresponding normal maps to highlight topological details.

Table 1. Quantitative comparison with other tokenization algorithms. Our Nautilus-style tokenization achieves more efficient compression while better preserving the proximity of neighboring vertices in the sequence.

Metrics	AMT [2024c]	EdgeRunner [2024]	Ours
Comp. Ratio \downarrow	0.462	0.474	0.275
Local Ratio \uparrow	0.378	0.461	0.554

sequence length relative to the original representation $9N$. Higher compression ratios enable modeling of meshes with more faces and better topological complexity. (2) **Local Ratio**, a new metric that we introduce, quantifies structural coherence among neighboring tokens. For each vertex, we calculate the proportion of its neighboring vertices in the mesh that appear within 100 preceding positions in the sequence. Higher local ratios indicate better preservation of local dependencies after serialization. In Table 1, our tokenization significantly outperforms other methods in both metrics, which is attributed to the explicit locality modeling in its design. In contrast, AMT processes mesh faces in an order of elongated strips rather than interconnected local parts, neglecting local dependencies during tokenization, while EdgeRunner relies on the excessive introduction of specialized tokens, leading to suboptimal performance in both metrics.

Generation Performance. We compared our point cloud conditioned generation results with MeshAnything [Chen et al. 2024b] and MeshAnythingV2 [Chen et al. 2024c], on a high-quality test set of 500 samples collected using the same protocol as in our qualitative experiments. Following the settings of previous work [Tang et al. 2024], we evaluate overall reconstruction quality by uniformly sampling 1,024 points from the surfaces of both ground truth and

Table 2. Quantitative Comparison with latest open-source methods, where our Nautilus framework significantly outperform others in both condition fidelity and visual quality.

Methods	C.Dist. \downarrow	H.Dist. \downarrow	User Study \uparrow
MeshAnything [2024b]	0.133	0.293	10.27%
MeshAnythingV2 [2024c]	0.106	0.248	13.17%
Nautilus (Ours)	0.087	0.176	88.68%

predicted meshes, and computing the Chamfer Distance (C.Dist.) and Hausdorff Distance (H.Dist.) between the sampled point clouds. Lower distances between point sets indicate higher reconstruction accuracy and better fidelity to the input condition. In addition, we conducted a user study to assess the proportion of results that users find satisfactory, with further details provided in *Appendix*. In Table 2, Nautilus significantly outperforms previous approaches across all metrics, validating its effectiveness that is consistent with the qualitative analysis presented in Sec. 4.2.

4.4 Ablation and Discussion

To validate the effectiveness of our proposed Nautilus-style tokenization and the Dual-Stream Point Conditioner, we perform extensive ablation studies on the tokenization scheme and the local encoder in our conditioner, where an additional quantitative ablation comparison is presented in *Appendix*.

Tokenization Scheme. We evaluated two configurations to demonstrate the key components of our tokenization design: using only coordinate compression (*Comp. only*) and using only the Nautilus Shell representation (*Rep. only*). Fig. 8 compares these variants with our full version. *Comp. only* achieves a compression ratio of 0.549

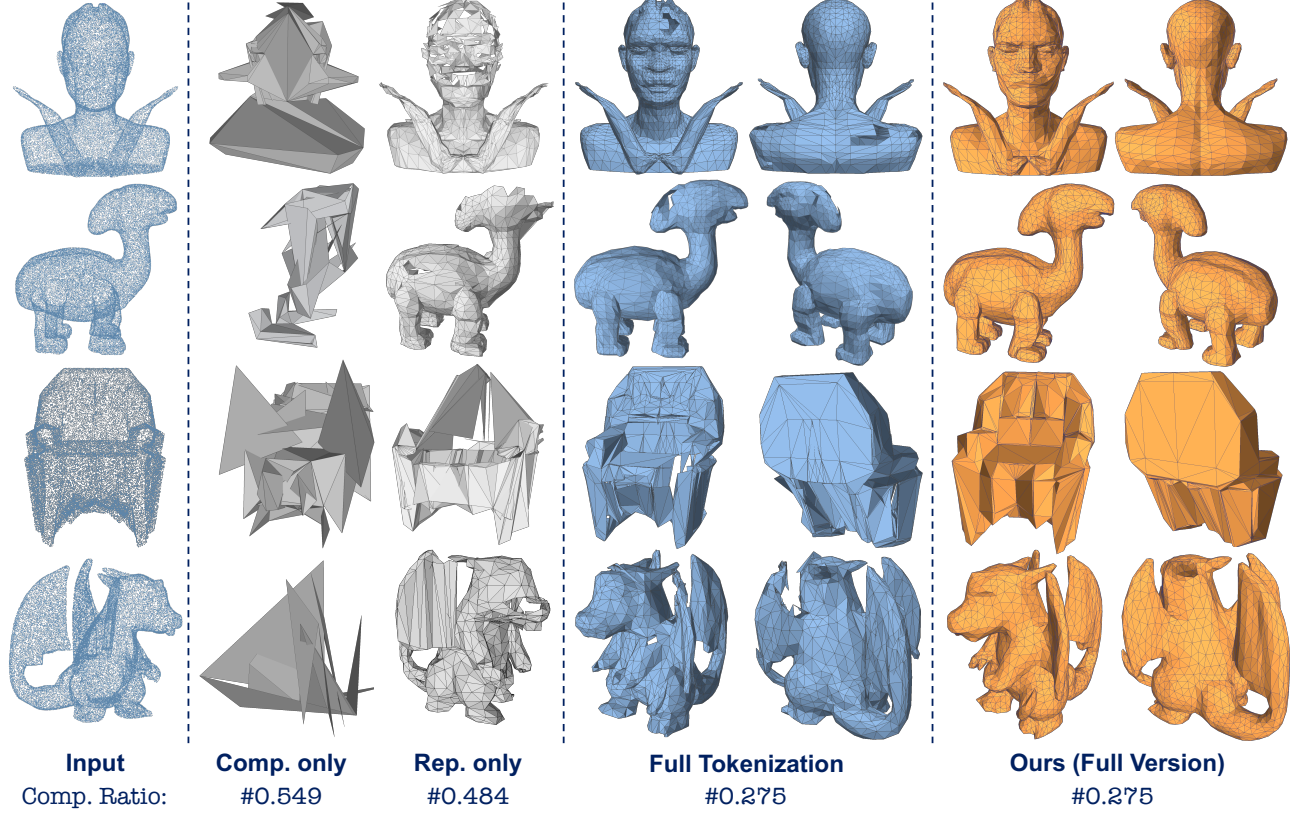


Fig. 8. We conduct ablation comparison on four specific configurations: using only the Coordinate Compression (*Comp. only*), using only the Nautilus Shell representation (*Rep. only*), using our *Full Tokenization* but without the local point encoder, and our *Full Version*.

and *Rep. only* achieves 0.484, both substantially higher than our full version’s 0.275. In terms of generation quality, *Comp. only* fails to construct the topology completely, while *Rep. only* produces a coarse outline of the target shape. In contrast, with the complete tokenization, our full version produces precisely structured results that are consistent with the input condition in geometry. With the explicit modeling of local neighboring vertices used in our Nautilus Shell representation, both *Rep. only* and our full version demonstrate better performance compared to *Comp. only*. In addition, as shown in the comparison among the two ablated groups and our full version, insufficient compression restricts the inclusion of complex training samples, leading to the model’s inability to learn intricate topologies effectively and resulting in generation failures.

Local Point Encoder. To evaluate the local encoder’s effectiveness in the point conditioner, we compare our full version with a variant that uses full tokenization but excludes the local encoder (*Full Tokenization*). As shown in Fig. 8, the variant without the local encoder exhibits minor manifold defects in complex topological regions, particularly surface holes in local structures. In contrast, our full version, which incorporates the local encoder, successfully resolves these issues and generates precise, compact meshes. The results demonstrate that the local geometric modeling provided by our local encoder yields significant improvements in local details

and connectivity, underscoring the importance of enhanced local dependency for generating precise local structures in challenging regions and mitigating manifold defects.

5 Conclusion and Future Works

In this paper, we present Nautilus, a locality-aware autoencoder designed for scalable high-fidelity mesh generation. By leveraging the locality of manifold meshes, Nautilus introduces a novel tokenization algorithm that preserves local dependency while achieving significant sequence compression, as well as a Dual-Stream Point Conditioner that enhances both global consistency and local structure fidelity. Our extensive experiments demonstrate that Nautilus outperforms state-of-the-art methods across various metrics, enabling the generation of meshes with unprecedented topological complexity and details. These results validate the importance of incorporating locality in tokenization and sequence prediction to achieve superior mesh generation. For future work, we aim to extend Nautilus to support broader 3D generation tasks, such as interactive scene editing and multi-object synthesis. Additionally, we plan to explore integrating multimodal conditioning, such as combining image, text, and point cloud inputs, to enhance the versatility of our framework. Another direction is to further optimize the efficiency of Nautilus to facilitate real-time applications.

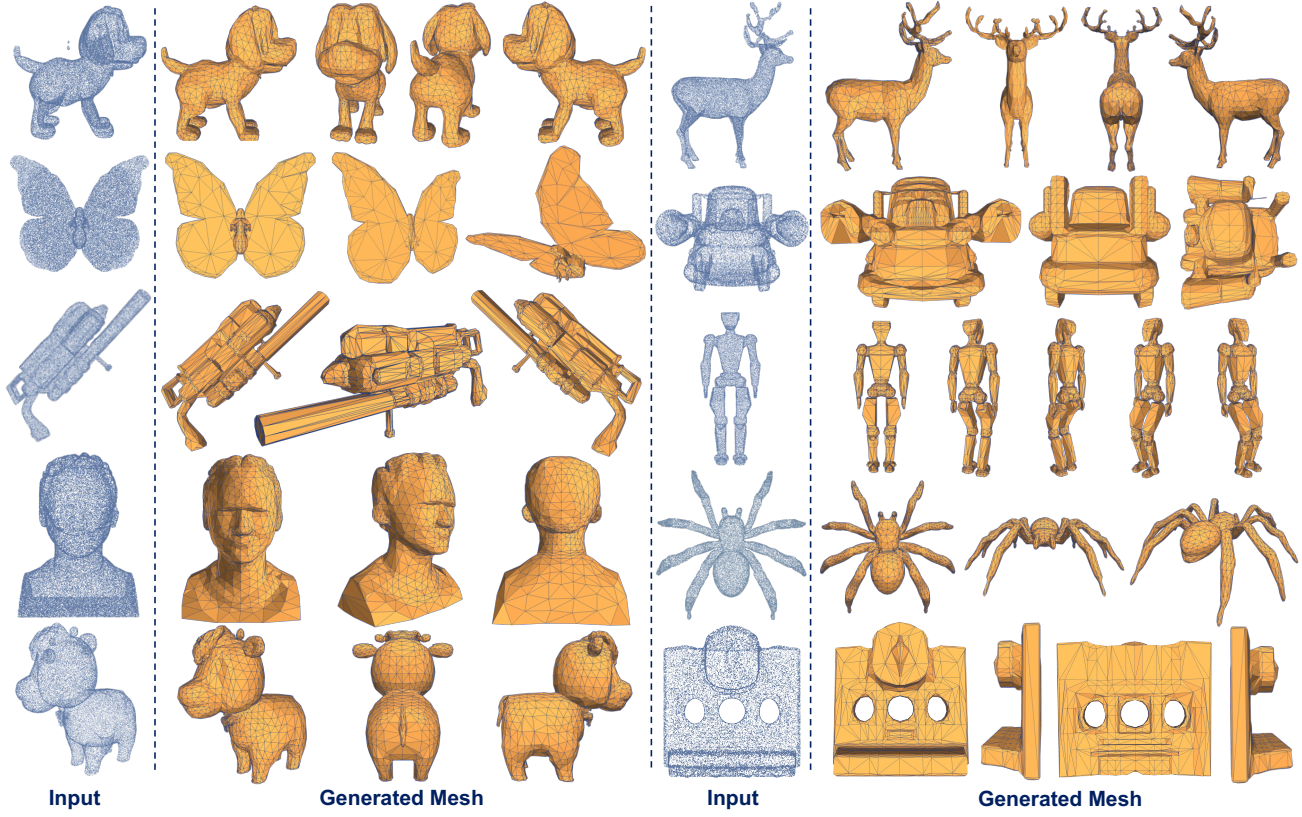


Fig. 9. We release additional point cloud conditioned generation results of our Nautilus across an extensive range of object categories.

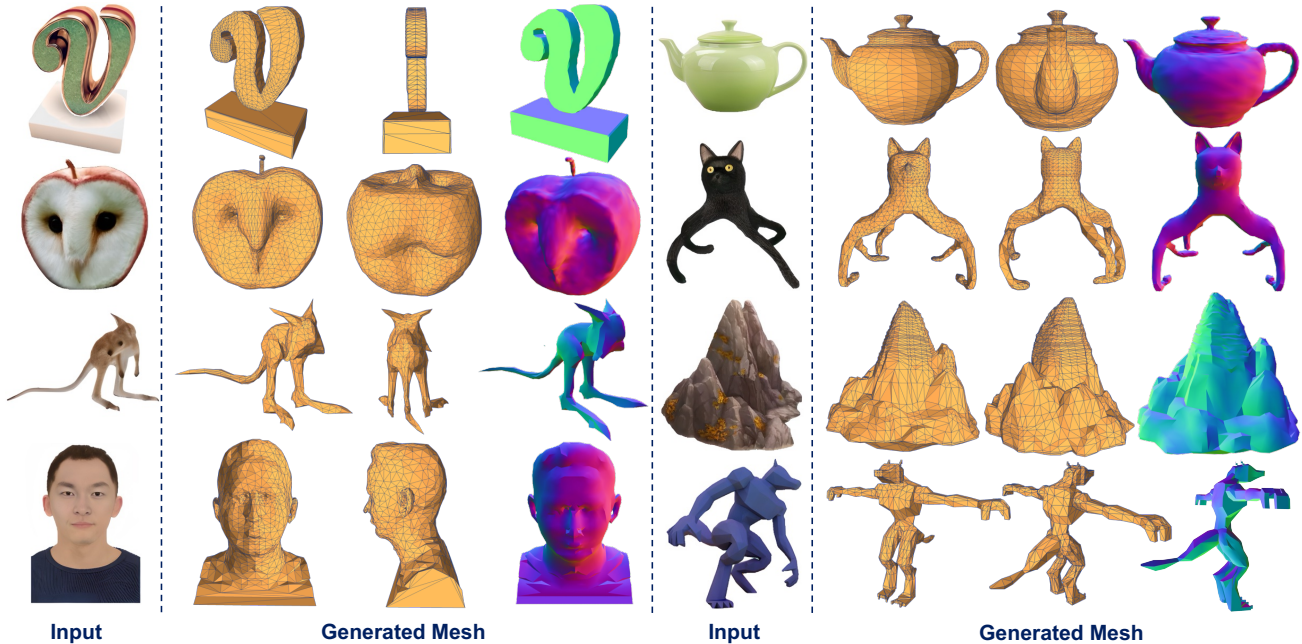


Fig. 10. We release additional image conditioned generation results of our Nautilus across an extensive range of object categories. The results are presented alongside corresponding normal maps to highlight the topology.

References

Antonio Alliegro, Yawar Siddiqui, Tatiana Tommasi, and Matthias Nießner. 2023. Polydiff: Generating 3d polygonal meshes with diffusion models. *arXiv preprint arXiv:2312.11417* (2023).

Marco Attene and Bianca Falcidieno. 2006. Remesh: An interactive environment to edit and repair triangle meshes. In *IEEE International Conference on Shape Modeling and Applications 2006 (SMI'06)*. IEEE, 41–41.

Jinbin Bai, Zhen Dong, Aosong Feng, Xiao Zhang, Tian Ye, and Kaicheng Zhou. 2023. Integrating view conditions for image synthesis. *arXiv preprint arXiv:2310.16002* (2023).

Jinbin Bai, Tian Ye, Wei Chow, Enxin Song, Qing-Guo Chen, Xiangtai Li, Zhen Dong, Lei Zhu, and Shuicheng Yan. 2024. Meissonic: Revitalizing masked generative transformers for efficient high-resolution text-to-image synthesis. *arXiv preprint arXiv:2410.08261* (2024).

Andrew Brock, Theodore Lim, James M Ritchie, and Nick Weston. 2016. Generative and discriminative voxel modeling with convolutional neural networks. *arXiv preprint arXiv:1608.04236* (2016).

Sijin Chen, Xin Chen, Anqi Pang, Xianfang Zeng, Wei Cheng, Yijun Fu, Fukun Yin, Yanru Wang, Zhibin Wang, Chi Zhang, et al. 2024a. MeshXL: Neural Coordinate Field for Generative 3D Foundation Models. *arXiv preprint arXiv:2405.20853* (2024).

Yiwen Chen, Tong He, Di Huang, Weicai Ye, Sijin Chen, Jiaxiang Tang, Xin Chen, Zhongang Cai, Lei Yang, Gang Yu, et al. 2024b. MeshAnything: Artist-Created Mesh Generation with Autoregressive Transformers. *arXiv preprint arXiv:2406.10163* (2024).

Yiwen Chen, Yikai Wang, Yihao Luo, Zhengyi Wang, Zilong Chen, Jun Zhu, Chi Zhang, and Guosheng Lin. 2024c. Meshanything v2: Artist-created mesh generation with adjacent mesh tokenization. *arXiv preprint arXiv:2408.02555* (2024).

Jaeyoung Chung, Suyoung Lee, Hyeongjin Nam, Jaerin Lee, and Kyoung Mu Lee. 2023. Luciddreamer: Domain-free generation of 3d gaussian splatting scenes. *arXiv preprint arXiv:2311.13384* (2023).

Angela Dai and Matthias Nießner. 2019. Scan2mesh: From unstructured range scans to 3d meshes. In *Proceedings of the IEEE/CVF Conference on Computer Vision and Pattern Recognition*. 5574–5583.

Patrick Esser, Sumeeth Kulal, Andreas Blattmann, Rahim Entezari, Jonas Müller, Harry Saini, Yam Levi, Dominik Lorenz, Axel Sauer, Frederic Boesel, et al. 2024. Scaling rectified flow transformers for high-resolution image synthesis. In *Forty-first International Conference on Machine Learning*.

Fangzhou Hong, Jiaxiang Tang, Ziang Cao, Min Shi, Tong Wu, Zhaoxi Chen, Shuai Yang, Tengfei Wang, Liang Pan, Dahu Lin, et al. 2024. 3dtopia: Large text-to-3d generation model with hybrid diffusion priors. *arXiv preprint arXiv:2403.02234* (2024).

Yicong Hong, Kai Zhang, Jiuxiang Gu, Sai Bi, Yang Zhou, Difan Liu, Feng Liu, Kalyan Sunkavalli, Trung Bui, and Hao Tan. 2023. Lrm: Large reconstruction model for single image to 3d. *arXiv preprint arXiv:2311.04400* (2023).

Michael Kazhdan, Matthew Bolitho, and Hugues Hoppe. 2006. Poisson surface reconstruction. In *Proceedings of the fourth Eurographics symposium on Geometry processing*. Vol. 7.

Weiyu Li, Jiarui Liu, Rui Chen, Yixun Liang, Xuelin Chen, Ping Tan, and Xiaoxiao Long. 2024b. CraftsMan: High-fidelity Mesh Generation with 3D Native Generation and Interactive Geometry Refiner. *arXiv preprint arXiv:2405.14979* (2024).

Zongming Li, Tianheng Cheng, Shoufa Chen, Peize Sun, Haocheng Shen, Longjin Ran, Xiaoxin Chen, Wenyu Liu, and Xinggang Wang. 2024a. Controlar: Controllable image generation with autoregressive models. *arXiv preprint arXiv:2410.02705* (2024).

Chen-Hsuan Lin, Jun Gao, Luming Tang, Towaki Takikawa, Xiaohui Zeng, Xun Huang, Karsten Kreis, Sanja Fidler, Ming-Yu Liu, and Tsung-Yi Lin. 2023. Magic3d: High-resolution text-to-3d content creation. In *Proceedings of the IEEE/CVF Conference on Computer Vision and Pattern Recognition*. 300–309.

William E Lorensen and Harvey E Cline. 1998. Marching cubes: A high resolution 3D surface construction algorithm. In *Seminal graphics: pioneering efforts that shaped the field*. 347–353.

Shitong Luo and Wei Hu. 2021. Diffusion probabilistic models for 3d point cloud generation. In *Proceedings of the IEEE/CVF conference on computer vision and pattern recognition*. 2837–2845.

Charlie Nash, Yaroslav Ganin, SM Ali Eslami, and Peter Battaglia. 2020. Polygon: An autoregressive generative model of 3d meshes. In *International conference on machine learning*. PMLR, 7220–7229.

Alex Nichol, Heewoo Jun, Prafulla Dhariwal, Pamela Mishkin, and Mark Chen. 2022. Point-e: A system for generating 3d point clouds from complex prompts. *arXiv preprint arXiv:2212.08751* (2022).

Jeong Joon Park, Peter Florence, Julian Straub, Richard Newcombe, and Steven Lovegrove. 2019. Deepsdf: Learning continuous signed distance functions for shape representation. In *Proceedings of the IEEE/CVF conference on computer vision and pattern recognition*. 165–174.

Ben Poole, Ajay Jain, Jonathan T Barron, and Ben Mildenhall. 2022. Dreamfusion: Text-to-3d using 2d diffusion. *arXiv preprint arXiv:2209.14988* (2022).

Xuanchi Ren, Jiahui Huang, Xiaohui Zeng, Ken Museth, Sanja Fidler, and Francis Williams. 2024. Xcube: Large-scale 3d generative modeling using sparse voxel hierarchies. In *Proceedings of the IEEE/CVF Conference on Computer Vision and Pattern Recognition*. 4209–4219.

Robin Rombach, Andreas Blattmann, Dominik Lorenz, Patrick Esser, and Björn Ommer. 2022. High-resolution image synthesis with latent diffusion models. In *Proceedings of the IEEE/CVF conference on computer vision and pattern recognition*. 10684–10695.

QiuHong Shen, Zike Wu, Xuanyu Yi, Pan Zhou, Hanwang Zhang, Shuicheng Yan, and XinChao Wang. 2024. Gamba: Marry gaussian splatting with mamba for single view 3d reconstruction. *arXiv preprint arXiv:2403.18795* (2024).

Yawar Siddiqui, Antonio Alliegro, Alexey Artemov, Tatiana Tommasi, Daniele Sirigatti, Vladislav Rosov, Angela Dai, and Matthias Nießner. 2024. Meshgpt: Generating triangle meshes with decoder-only transformers. In *Proceedings of the IEEE/CVF Conference on Computer Vision and Pattern Recognition*. 19615–19625.

Jiaxiang Tang, Zhaoxi Chen, Xiaokang Chen, Tengfei Wang, Gang Zeng, and Ziwei Liu. 2025. Lgm: Large multi-view gaussian model for high-resolution 3d content creation. In *European Conference on Computer Vision*. Springer, 1–18.

Jiaxiang Tang, Zhaoshuo Li, Zekun Hao, Xian Liu, Gang Zeng, Ming-Yu Liu, and Qingsheng Zhang. 2024. Edgerunner: Auto-regressive auto-encoder for artistic mesh generation. *arXiv preprint arXiv:2409.18114* (2024).

Jiaxiang Tang, Jiawei Ren, Hang Zhou, Ziwei Liu, and Gang Zeng. 2023. Dreamgaussian: Generative gaussian splatting for efficient 3d content creation. *arXiv preprint arXiv:2309.16653* (2023).

Tencent Hunyuan3D Team. 2025. Hunyuan3D 2.0: Scaling Diffusion Models for High Resolution Textured 3D Assets Generation.

Aaron Van Den Oord, Oriol Vinyals, et al. 2017. Neural discrete representation learning. *Advances in neural information processing systems* 30 (2017).

A Vaswani. 2017. Attention is all you need. *Advances in Neural Information Processing Systems* (2017).

Yuxuan Wang, Xuanyu Yi, Zike Wu, Na Zhao, Long Chen, and Hanwang Zhang. 2025. View-consistent 3d editing with gaussian splatting. In *European Conference on Computer Vision*. Springer, 404–420.

Zhengyi Wang, Cheng Lu, Yikai Wang, Fan Bao, Chongxuan Li, Hang Su, and Jun Zhu. 2024. Prolificdreamer: High-fidelity and diverse text-to-3d generation with variational score distillation. *Advances in Neural Information Processing Systems* 36 (2024).

Haohan Weng, Yikai Wang, Tong Zhang, CL Chen, and Jun Zhu. 2024. PivotMesh: Generic 3D Mesh Generation via Pivot Vertices Guidance. *arXiv preprint arXiv:2405.16890* (2024).

Jiajun Wu, Chengkai Zhang, Tianfan Xue, Bill Freeman, and Josh Tenenbaum. 2016. Learning a probabilistic latent space of object shapes via 3d generative-adversarial modeling. *Advances in neural information processing systems* 29 (2016).

Shuang Wu, Youtian Lin, Feihu Zhang, Yifei Zeng, Jingxi Xu, Philip Torr, Xun Cao, and Yao Yao. 2024a. Direct3D: Scalable Image-to-3D Generation via 3D Latent Diffusion Transformer. *arXiv preprint arXiv:2405.14832* (2024).

Zike Wu, Pan Zhou, Xuanyu Yi, Xiaoding Yuan, and Hanwang Zhang. 2024b. Consistent3d: Towards consistent high-fidelity text-to-3d generation with deterministic sampling prior. In *Proceedings of the IEEE/CVF Conference on Computer Vision and Pattern Recognition*. 9892–9902.

Jiale Xu, Weihao Cheng, Yiming Gao, Xintao Wang, Shenghua Gao, and Ying Shan. 2024. Instantmesh: Efficient 3d mesh generation from a single image with sparse-view large reconstruction models. *arXiv preprint arXiv:2404.07191* (2024).

Xuanyu Yi, Zike Wu, QiuHong Shen, Qingshan Xu, Pan Zhou, Joo-Hwee Lim, Shuicheng Yan, XinChao Wang, and Hanwang Zhang. 2024a. MVGamba: Unify 3D Content Generation as State Space Sequence Modeling. *arXiv preprint arXiv:2406.06367* (2024).

Xuanyu Yi, Zike Wu, Qingshan Xu, Pan Zhou, Joo-Hwee Lim, and Hanwang Zhang. 2024b. Diffusion time-step curriculum for one image to 3d generation. In *Proceedings of the IEEE/CVF Conference on Computer Vision and Pattern Recognition*. 9948–9958.

Biao Zhang, Matthias Nießner, and Peter Wonka. 2022. 3dilg: Irregular latent grids for 3d generative modeling. *Advances in Neural Information Processing Systems* 35 (2022), 21871–21885.

Chubin Zhang, Hongliang Song, Yi Wei, Yu Chen, Jiwen Lu, and Yansong Tang. 2024a. Geolrm: Geometry-aware large reconstruction model for high-quality 3d gaussian generation. *arXiv preprint arXiv:2406.15333* (2024).

Longwen Zhang, Ziyu Wang, Qixuan Zhang, Qiwei Qiu, Anqi Pang, Haoran Jiang, Wei Yang, Lan Xu, and Jingyi Yu. 2024b. CLAY: A Controllable Large-scale Generative Model for Creating High-quality 3D Assets. *ACM Transactions on Graphics (TOG)* 43, 4 (2024), 1–20.

Zibo Zhao, Wen Liu, Xin Chen, Xianfang Zeng, Rui Wang, Pei Cheng, Bin Fu, Tao Chen, Gang Yu, and Shenghua Gao. 2024. Michelangelo: Conditional 3d shape generation based on shape-image-text aligned latent representation. *Advances in Neural Information Processing Systems* 36 (2024).

Linqi Zhou, Yilun Du, and Jiajun Wu. 2021. 3d shape generation and completion through point-voxel diffusion. In *Proceedings of the IEEE/CVF international conference on computer vision*. 5826–5835.

A Step-by-Step Demonstration of Our Tokenization

In our main paper, we design a novel Nautilus-style Tokenization algorithm that preserves local dependency while achieving effective sequence length compression. In Algorithm 1, we provide a step-by-step demonstration of our tokenization algorithm, including the initial sorting of vertices and faces, shell construction by vertices traversal, and the coordinates compression of traversed vertices.

Algorithm 1 Step-by-Step Pipeline of Nautilus-Style Tokenization

```

1: Input: manifold mesh asset  $\mathcal{M} = (\mathcal{V}, \mathcal{F})$  consisting of vertices  $\mathcal{V} = \{v_i\}$  and faces  $\mathcal{F} = \{f_i\}$ .
2: Sort vertices  $\mathcal{V}$  by their  $z \cdot y \cdot x$  coordinates.
3: Sort faces  $\mathcal{F}$  by the smallest vertex index in each face.
4: Initialize a list of unvisited faces  $U_f \leftarrow \mathcal{F}$ .
5: Compute the degree  $\deg(v_i)$  for all  $v_i \in \mathcal{V}$ , where  $\deg(v_i)$  represents the number of edges connected to vertex  $v_i$ .
6: Select the highest-degree vertices in the first face  $f_1 \in U_f$  as the initial center  $O_1$ .
7: Initialize the tokenized sequence  $S(\mathcal{M}) \leftarrow \emptyset$  and set shell index  $k \leftarrow 1$ .
8: while  $U_f \neq \emptyset$  do:
9:   Identify all faces in  $U_f$  that contain  $O_k$ .
10:  Sort these faces in adjacent order, extract their surrounding vertices  $\{P_{k,i}\}$ .
11:  Extend  $S(\mathcal{M}) \leftarrow S(\mathcal{M}) \cup \{O_k, P_{k,1}, \dots, P_{k,\text{end}}\}$ , completing shell  $k$ .
12:  Identify all neighbor vertices of  $P_{k,\text{end}}$ , denoted as  $\mathcal{N}(P_{k,\text{end}}) = \{N_{k,\text{end}}^i\}$ .
13:  Find the vertex with the maximum degree:

$$N_{k,\text{end}}^{\max} = \arg \max_{N \in \mathcal{N}(P_{k,\text{end}})} \deg(N).$$

14:  If  $\deg(N_{k,\text{end}}^{\max}) > 4$  (to ensure at least three connected faces in the next shell):
15:    Set  $O_{k+1} \leftarrow N_{k,\text{end}}^{\max}$ .
16:  Else:
17:    Set  $O_{k+1}$  as highest-degree vertex in the first remaining face  $f_1 \in U_f$ .
18:    Update  $\deg(v_i)$  for all  $v_i \in \mathcal{V}$  to reflect the remaining unvisited edges.
19:    Remove all visited faces from  $U_f$ ,  $k \leftarrow k + 1$ .
20: Convert the discrete coordinates  $(x, y, z) \in \mathbb{R}^{128}$  of vertices in  $S(\mathcal{M})$  to  $(u, v)$ .
21: Flatten the vertices represented in  $(u, v)$  coordinates to 1D sequence.
22: Codebook mapping  $S(\mathcal{M})$ :  $u_k^P = u_k^P, v = v + 1024, u_k^Q = u_k^Q + 1024 + 2048$ , where 1024 is the codebook size of  $u_k^P$  and 2048 is the codebook size of  $v$ .
23: Output: Tokenized sequence  $S(\mathcal{M})$ .

```

B Extensive Experiments and Analysis

Our experiments in the main paper comprehensively evaluate the effectiveness of **Nautilus**. In this section, we provide supplementary analysis and discussion to explore behind its efficacy:

- Sec.B.1: We present an additional quantitative ablation study to complement the qualitative ablation comparisons in the main paper.
- Sec.B.2: We exclusively examine the impact of local dependency on tokenization representation by comparing our Nautilus Shell representation with an upgraded version of the AMT representation that equips our coordinate compression.
- Sec.B.3: We analyze the modeling of local dependency by visualizing the attention maps in the transformer decoder.
- Sec.B.4: We discuss the influence of sequence length on the model’s generation capability.

B.1 Quantitative Ablation Study

In our main paper, we conduct a qualitative ablation study on point-cloud-conditioned generation. Here, we extend the analysis to a quantitative evaluation on the same high-quality test set of 500 samples used in our main paper. In Table 3, we compare four configurations: using only the Coordinate Compression (*Comp. only*), using only the Nautilus Shell Representation (*Rep. only*), using our *Full Tokenization* but without the local encoder, and our *Full Version*.

To assess the generation quality, we follow a similar evaluation protocol: uniformly sampling 1,024 points from the surfaces of both the ground truth and generated meshes. The Chamfer Distance (C.Dist.) and Hausdorff Distance (H.Dist.) are then computed between these sampled point sets to quantify the reconstruction accuracy. Lower values of these metrics indicate a closer alignment between the predicted and ground truth meshes, reflecting higher fidelity to the input conditions.

Table 3. We conduct quantitative ablation comparison on four specific configurations: using only the Coordinate Compression (*Comp. only*), using only the Nautilus Shell Representation (*Rep. only*), using our *Full Tokenization* but without the local encoder, and our *Full Version*.

Ablation	Comp. only	Rep. only	Full Tokenization	Full Version
C.Dist. \downarrow	0.151	0.100	0.092	0.087
H.Dist. \downarrow	0.355	0.213	0.186	0.176

As shown in Table 3, our findings are consistent with the qualitative ablation study, confirming that the *Full Version* outperforms all ablated configurations. Notably, the Nautilus Shell representation provides the most substantial improvement (see *Rep. only* vs. *Comp. only*), while Coordinate Compression further contributes to the mesh quality (see *Full Tokenization* vs. *Rep. only*). Additionally, the inclusion of our Local Encoder in the conditioner offers a significant performance boost (see *Full Tokenization* vs. *Full Version*). Our findings confirm that achieving both compression and preservation of local dependency, as implemented in our Nautilus, is essential to generate high-quality meshes.

B.2 Ablated Comparison with AMT Representation

To further investigate the influence of **local dependency preservation** of tokenization algorithms on generation quality, we perform additional experimental comparisons between our Nautilus Shell representation and the AMT in MeshAnythingV2, while excluding the influence of different training data and compression ratio.

Specifically, we apply the same coordinate compression to the AMT representation and train it on the same dataset as Nautilus, enabling it to model more than 5,000 faces. In Fig. 11, we denote the improved AMT version as *AMT Comp.*, comparing it with our full version on challenging samples with complex topology and rich geometric details. Despite achieving a compression ratio comparable to that of Nautilus, *AMT Comp.* still exhibits severe manifold defects in its generation results, particularly **isolated strips** consisting of single-line faces.

This issue arises from the lack of local dependency preservation in AMT’s traversal. Unlike the part-by-part approach taken by human artists, AMT processes mesh faces in elongated strips, making it extremely challenging for the model to precisely connect these strips into manifold meshes. Without preserving local dependency, for each face in the sequential generation, its neighboring faces in the mesh are often located far apart in the sequence. This requires the decoder to build highly precise features to globally align and gather information from these distant neighbors. As these neighbors are essential for determining the shape of the current face according to

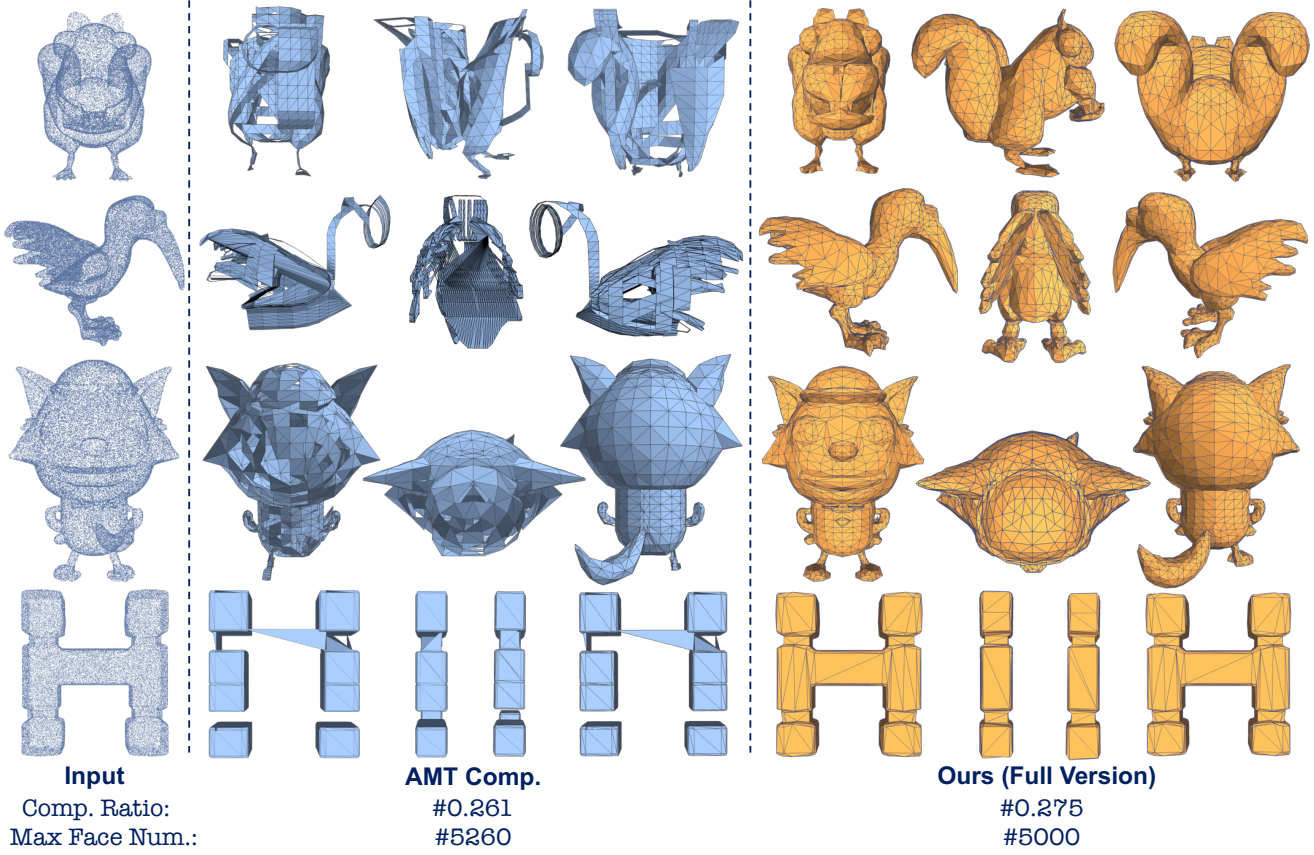


Fig. 11. Ablated comparison of generated results between the representation of AMT and our Nautilus Shell representations. To independently analyze the influence of local dependency preservation, both groups are trained on the same dataset, and AMT is improved by incorporating the same coordinate compression as Nautilus to achieve a comparable number of faces, denoted as *AMT Comp.*

mesh locality, failing to aggregate their information leads to poor interconnections and manifold defects.

In contrast, Nautilus preserves short-distance, local dependency, maintaining the proximity of spatially neighboring vertices in the tokenized sequence. During the generation of each face, this local dependency introduces an inductive bias, facilitating the decoder to simply gather information from nearby positions in the sequence. This approach enables Nautilus to achieve significantly better local interconnection and structural fidelity. Our results highlight the importance of preserving local dependency in tokenization algorithms for generating high-quality meshes. Additional visualization analysis is provided in Sec. B.3.

B.3 Visualized Analysis on Local Dependency

In Supp. Sec. B.2, we conducted additional ablation comparisons to demonstrate the significance of preserving local dependency within tokenization algorithms. In this section, we present a visualized analysis to directly examine the modeling of local dependency. Specifically, we compare the averaged attention maps of our Nautilus and that of the ablated group *AMT Comp.* designed in Supp.

Sec. B.2. For each model, we compute the averaged causal attention map across 50 samples and all 24 self-attention layers in the transformer decoder, in order to evaluate the models’ capacity to model local dependency.

We present our findings in Fig.12, where each row represents a query (Q) position and each column represents a key (K) position. Bright colors indicate stronger attention weights directed from a Q position to a K position. From Fig.12, it is evident that Nautilus exhibits highly concentrated bright regions close to the diagonal. In other words, for each query position, the attention is predominantly focused on a few nearby positions within the sequence. In contrast, the attention map of *AMT Comp.* shows more dispersed bright regions, suggesting that attention is distributed to positions farther away in the sequence compared to Nautilus. This visualization clearly demonstrates the impact of local dependency preservation on the performance of decoder. By effectively maintaining the proximity of spatially neighboring vertices in the tokenized sequence, the transformer decoder in Nautilus gathers local topology information more efficiently from nearby positions within the sequence, which contributes to its superior quality of generation.

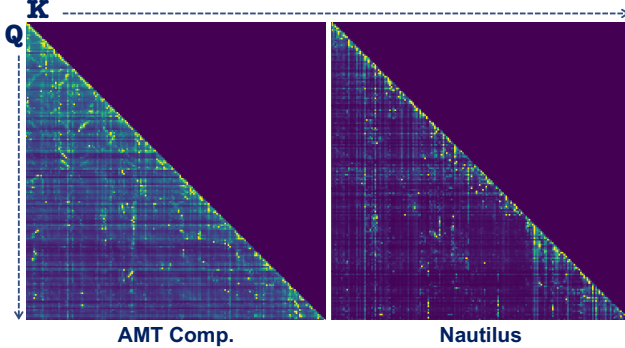


Fig. 12. Comparison of averaged Attention Maps between *AMT Comp.* and *Nautilus*. The attention maps are averaged over 50 samples and all 24 self-attention layers in the decoder. Each row corresponds to a query (Q) position, and each column corresponds to a key (K) position. Bright colors indicate stronger attention weights directed from a Q position to a K position.

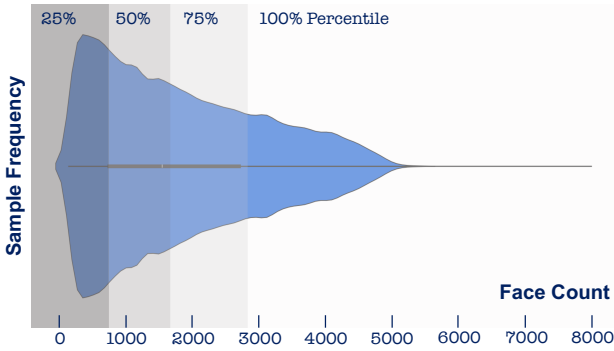


Fig. 13. Statistics on the face counts of samples in our training set, comprising 311K high-quality mesh assets with up to 8,000 faces.

B.4 Discussion on Sequence Length

In this section, we provide a comprehensive discussion on how compression ratio directly impacts generation quality during both training and inference stages.

Effect in Training. During training, artist-created mesh assets in the dataset are converted into sequences through tokenization. Due to GPU memory limits, the maximum sequence length of a 500M parameter transformer decoder in autoregressive mesh generation is typically around 20,000. For efficient training, sequence lengths are generally constrained under 15,000. Within this limit, tokenization algorithms with higher compression ratios enable the inclusion of more complex, high-face-count mesh assets. Learning from such assets enables the model to handle complex geometries under challenging conditions, mitigating failures such as missing components, large surface holes, and other structural defects. With *Nautilus* achieving an unprecedented compression ratio of 0.275, it allows the inclusion of mesh assets containing over 5,000 faces

in 12,000 tokens. This compression facilitates the model’s ability to learn from high-quality assets, enabling the generation of unprecedented topological complexity.

Effect in Inference. The inherent gap between the prediction of the next token during training and autoregressive inference during inference amplifies the cumulative errors as the length of the sequence increases. Our empirical analysis reveals that, even with well-optimized models, the validation loss at the 15,000-th position is approximately three times higher than at the 5,000-th position. Therefore, tokenization algorithms with lower compression ratios further aggravate this issue by requiring longer sequences to represent the same number of faces, increasing the likelihood of defects. This observation aligns with our ablation study, where the groups using only *Nautilus Shell Representation* (*Rep. Only*) demonstrates inferior generation quality compared to the *Full Tokenization*, which is attributed to its inferior compression ability.

C Further Statistics in this Work

C.1 Training Data Statistics

We conducted a statistical analysis of the face counts in our training dataset, with the results shown in Fig. 13. Our training dataset consists of 311K high-quality mesh assets that can be tokenized into 12,000-length sequences using our *Nautilus*-style Tokenization Algorithm. As illustrated in the figure, about 50% of the samples exceed the maximum face count of 1,600 supported by previous methods and even include a small subset of extremely complex samples with 5,000 to 8,000 faces. This demonstrates that our tokenization method, while typically supporting meshes with up to 5,000 faces, is capable of achieving an even higher level of compression in certain cases, enabling the tokenization of meshes with up to 8,000 faces. Leveraging this extensive and carefully curated training set, which covers a wide range of face counts, *Nautilus* not only ensures basic geometric modeling but also learns the ability to effectively handle complex topologies.

C.2 User Study Statistics

In this section, we provide additional details of our User Study. As shown in Fig. 14, each question in our study includes the rendering visualizations of the input point cloud and the output meshes generated by the compared methods. To ensure unbiased feedback, all options are presented anonymously, and their order is shuffled for every question. Specifically, users are asked to evaluate each result by indicating whether they are satisfied with it. For each method, we collect the responses and calculate the average satisfaction rates across all questions. In total, our User Study consists of 20 questions, featuring 20 input point clouds and 60 corresponding mesh assets generated from the three comparing methods. In total, the survey received 38 responses from participants with diverse backgrounds. This carefully designed questionnaire, combined with a broad participant base, ensures the objectivity and reliability of the results.

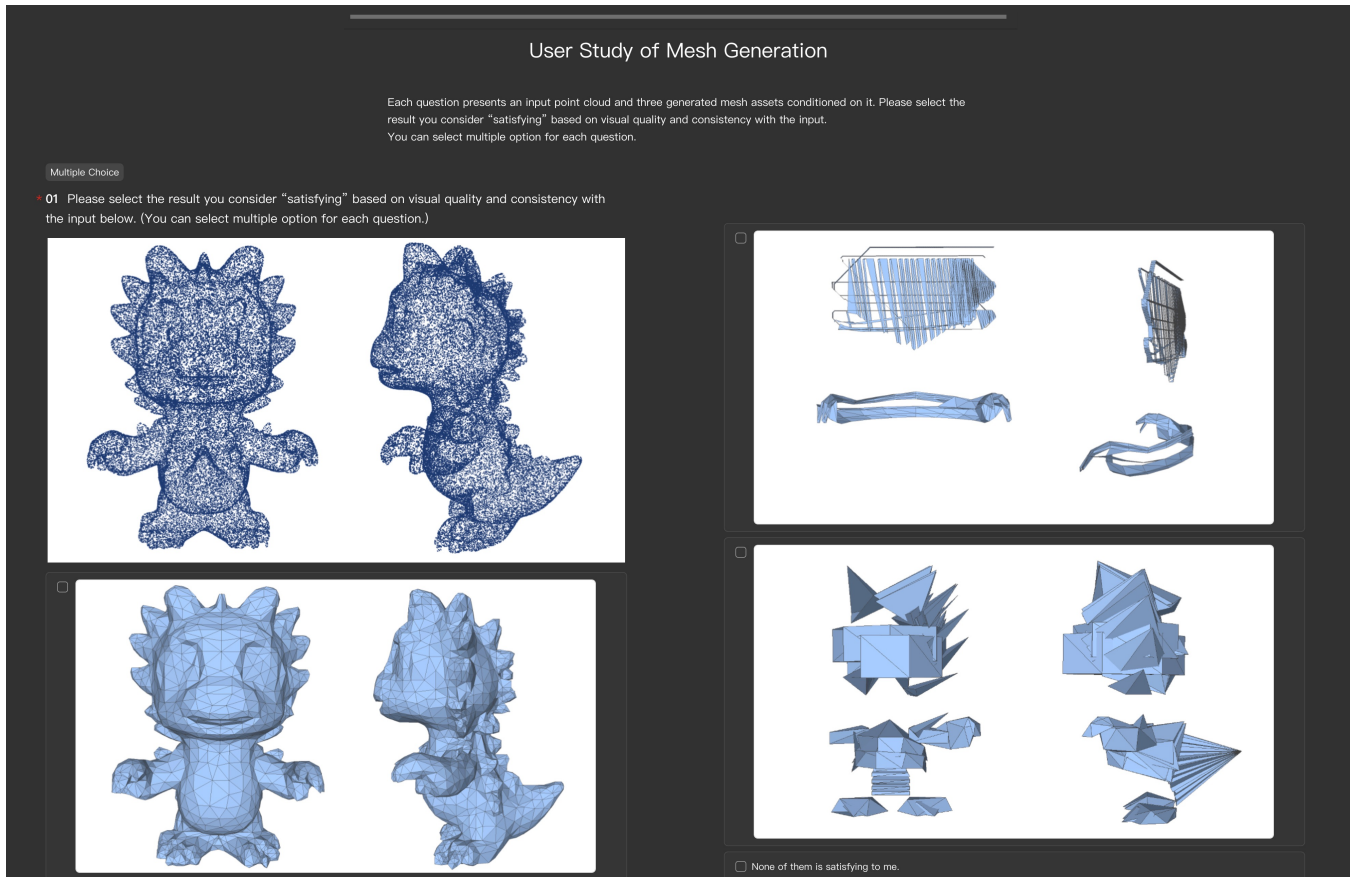


Fig. 14. The Interface of Our User Study. Given the rendered images of the input condition and the generated meshes from each compared method, users are asked to indicate whether they are satisfied with each result. For each method, we calculate the average satisfaction rate across all samples.